Connecting Quantum Cities: Simulation of a Satellite-Based Quantum Network

Raja Yehia, Matteo Schiavon, Valentina Marulanda Acosta, Tim Coopmans, Iordanis Kerenidis, David Elkouss, Eleni Diamanti

New Journal of Physics
The open access journal at the forefront of physics

Deutsche Physikalische Gesellschaft DPG IOP Institute of Physics

PAPER • OPEN ACCESS

Connecting quantum cities: simulation of a satellite-based quantum network

To cite this article: Raja Yehia *et al* 2024 *New J. Phys.* **26** 073015

IOP Publishing New J. Phys. 26 (2024) 073015 https://doi.org/10.1088/1367-2630/ad5b13

New Journal of Physics
The open access journal at the forefront of physics

Deutsche Physikalische Gesellschaft DPG
IOP Institute of Physics

Published in partnership with: Deutsche Physikalische Gesellschaft and the Institute of Physics

OPEN ACCESS

RECEIVED
26 February 2024

REVISED
28 March 2024

ACCEPTED FOR PUBLICATION
23 June 2024

PUBLISHED
9 July 2024

PAPER

Connecting quantum cities: simulation of a satellite-based quantum network

Raja Yehia[1,2,3,*], **Matteo Schiavon**[1], **Valentina Marulanda Acosta**[1,4], **Tim Coopmans**[5,6], **Iordanis Kerenidis**[2], **David Elkouss**[5,7] and **Eleni Diamanti**[1]

[1] Sorbonne Université, CNRS, LIP6, F-75005 Paris, France
[2] Université de Paris, CNRS, IRIF, F-75013 Paris, France
[3] ICFO—Institut de Ciencies Fotoniques, The Barcelona Institute of Science and Technology, Casteldeffels, Spain
[4] DOTA, ONERA, Université Paris Saclay, F-92322 Châtillon, France
[5] QuTech, Delft University of Technology, Lorentzweg 1, 2628 CJ Delft, The Netherlands
[6] Leiden Institute of Advanced Computer Science, Leiden University, Niels Bohrweg 1, 2333 CA Leiden, The Netherlands
[7] Networked Quantum Devices Unit, Okinawa Institute of Science and Technology Graduate University, Okinawa, Japan
[*] Author to whom any correspondence should be addressed.

E-mail: raja.yehia@icfo.net

Keywords: simulations, satellite-based, networks, QKD, free-space, quantum communication

Abstract

We present and analyze an architecture for a European-scale quantum network using satellite links to connect Quantum Cities, which are metropolitan quantum networks with minimal hardware requirements for the end users. Using NetSquid, a quantum network simulation tool based on discrete events, we assess and benchmark the performance of such a network linking distant locations in Europe in terms of quantum key distribution rates, considering realistic parameters for currently available or near-term technology. Our results highlight the key parameters and the limits of current satellite quantum communication links and can be used to assist the design of future missions. We also discuss the possibility of using high-altitude balloons as an alternative to satellites.

1. Introduction

The promises of the Quantum Internet, a global network of quantum devices connected through quantum channels [1], are numerous. Such an infrastructure can enhance the performance of current networks by increasing their security or communication efficiency [2–5], allows for new functionalities such as, for instance, secure delegated computing [6, 7], and opens the way to distributed quantum computing and sensing [8, 9]. Quantum network protocols between two or multiple parties [10–13] executed over the Internet require quantum states to be transferred across the infrastructure, typically in the form of shared entanglement. This is achieved by routing quantum states through the network via teleportation, which consumes the entanglement of so-called Bell (or EPR) pairs [14, 15]. The ability to efficiently share entanglement between any number of remote nodes of the network is therefore a fundamental resource for Quantum Internet applications and currently the topic of intense efforts aiming at optimal network architecture designs [16].

While increasingly advanced quantum networks are being deployed [17, 18], it becomes crucial to consider more global strategies for connecting metropolitan or regional scale networks to reach continental scales and beyond. Carefully developed simulation tools can be extremely helpful to this end, and can inform the design of both near and longer term quantum networks, in particular at the present stage of small scale deployment, where it is desirable to avoid wasting resources on ultimately unscalable architectures.

One of the main obstacles towards building an international quantum network is long distance communication. After a few tens of kilometers, photon loss in fiber becomes predominant and prevents practical applications. Well known bounds [19, 20] give fundamental limits on quantum communication over long distance in a fiber. Quantum repeaters [21–24], the quantum analogues of signal amplifiers in

classical networks, will provide a solution to this problem. However, despite significant experimental advances in the recent past [24–27], they do not have yet the necessary technological maturity [28–30]. Over the last decade, free space communication and more particularly satellite communication has received more and more attention as a complementary solution to overcome this issue. Feasibility studies [31, 32], together with experimental implementations of ground-to-ground [33], airplane-to-ground [34] or balloon-to-ground [35] free-space channels, have led the way to some experimental studies of satellite-to-ground quantum communication exploiting a simulated quantum source on satellite [36, 37]. A crucial milestone in the race for satellite communication was the launch of the Chinese satellite Micius [38], which has allowed for the first demonstration of prepare-and-measure [39] and entanglement-based [40] quantum key distribution (QKD) and of other quantum protocols, such as quantum teleportation [41], using a satellite terminal. In satellite communication, the main source of loss is given by diffraction, which scales quadratically with the distance, in stark contrast with the exponential loss in glass fiber. Satellite quantum communication thus appears as a particularly appealing choice for interconnecting the metropolitan quantum networks under deployment, as demonstrated by the QKD network deployed in China, which extends over more than 4000 km [18].

Considering that the use of satellite links will play a central role in the implementation of very large scale quantum networks, the design of a complete network infrastructure requires a way to simulate such links, including in particular atmospheric perturbations. Previous works have mostly focused on integrated models of a single passage of a satellite above two ground stations, where the atmospheric effects are modeled in an aggregated way through an average transmissivity, which moreover only takes into account attenuation and diffraction losses [42, 43], or also the beam-wandering effects due to atmospheric turbulence and pointing error [44]. All these works consider a downlink channel, with the source on the satellite and the detectors in the ground station. This is justified by the fact that most of the travelling of the photons happens in space, where there is no atmosphere and the only loss and noise are due to diffraction; the fact that the atmosphere affects the beam only in the last part of the channel gives a lower beam-wandering effect than in the uplink case, where these effects are at the beginning of the propagation. For this reason, in this work we will also concentrate on the downlink scenario.

However, contrary to previous works, we consider an atmospheric model that provides, for each photon traveling through the channel, the instantaneous value of the transmissivity. Considering the effect of transmission at each point of the satellite is relevant for the performance of satellite quantum communication because the distance between the satellite and the ground stations is not constant and also due to the limited time window during which a satellite is in view of a ground station. In this work, we quantify this effect by simulating each photon, emitted from a moving satellite, individually.

Our simulation tool is based on NetSquid [45, 46], a quantum network simulator with discrete events developed at QuTech in the Netherlands. We have previously developed using NetSquid a set of subroutines allowing the simulation of a metropolitan terrestrial quantum network, with which we studied the feasibility of different protocols [47]. Here, we add satellite nodes, noise models relevant for satellite to ground links and routines to simulate satellite orbits. The code used in our work is available on GitHub [48, 49].

We use these tools to investigate the feasibility of a satellite-based network architecture in a realistic context within Europe. We show our envisioned network architecture that we call the Qloud in figure 1. In this architecture, users with minimal quantum technology abilities, called Qlients, are connected to central nodes called Qonnectors, together forming a star network which we refer to as Quantum City. In turn, the Qonnectors are connected to other Qonnectors through a network of bacQbone nodes, thereby enabling quantum communication between any two users in the network. This setup is very general to allow putting as few restrictions as possible on potential future extensions or applications, while minimizing the hardware requirements on the end users. This is key for practical implementations. In this work, we investigate quantum communication between Quantum Cities based on satellite links acting as bacQbone nodes between Qonnectors.

We investigate a small Qloud with simulations using real satellite data that show the feasibility of QKD in this network. QKD is one of the most studied applications of quantum communication and we use it here as a performance benchmark for the network under study. We first examine the critical parameters of satellite quantum communication by looking separately at their effect on the key rate in a simple BB84 downlink scenario. Then, we analyze and discuss the practical relevance of such links in different realistic network settings. More precisely this work is organized as follows. After briefly recalling the characteristics of a Quantum City in section 2, we detail our model for simulating satellite quantum communication to connect Quantum Cities. Then in section 3 we focus on a simple downlink scenario and employ our simulation code for an exploratory case: first, we determine a suitable satellite which we choose for later investigations, and then we characterize the influence of the various parameters in our model. In section 4, we embed this study

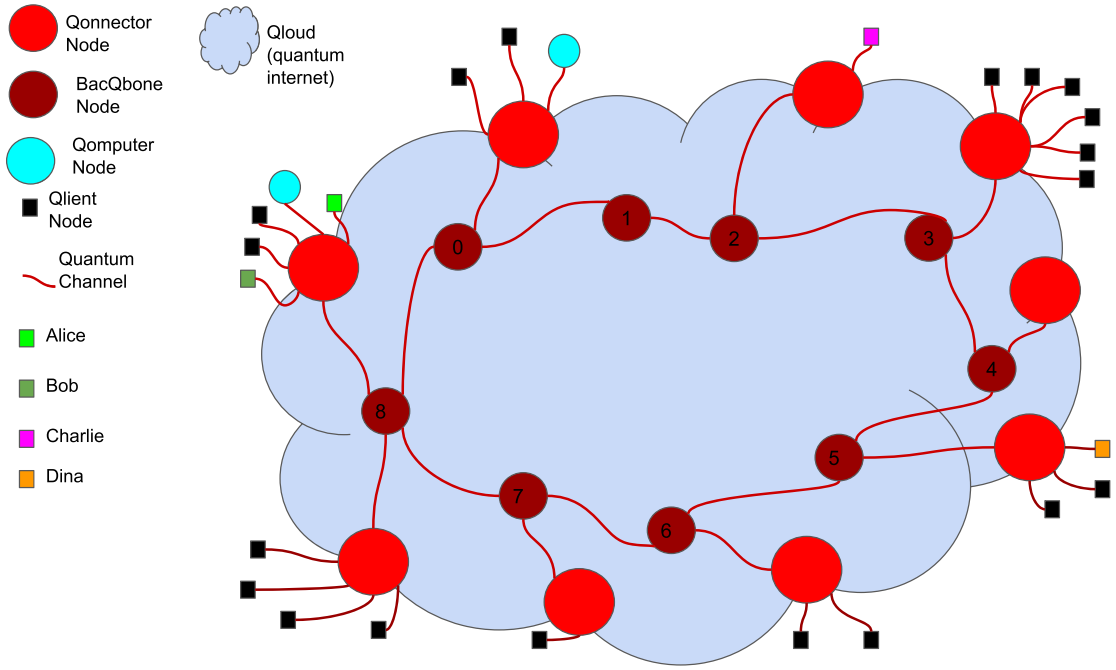

Figure 1. Schematic of a Qloud: Quantum Cities connected through a backbone network of satellites (bacQbone nodes). A Quantum City is formed by a powerful central node (Qonnector) used as a server allowing end users (Qlients) to enjoy quantum-enhanced functionalities. The end users can also be powerful quantum machines (Qomputer nodes).

in the context of quantum networks and obtain the achievable raw QKD rate between two distant users in different settings. Finally, in section 5, we use these results to discuss the perspectives of satellite quantum communication in the near future as well as some alternatives such as the use of high-altitude balloons, which has seen a rising interest in the last few years [50–52].

2. Architecture description

2.1. Quantum City

In previous work [47], we introduced the Quantum City architecture for metropolitan photonic quantum networks that minimizes the hardware necessary for the users while still enhancing current classical networks. In this section, we recall the main features of this architecture.

Our model considers a star topology with a central node, that we call Qonnector, linked to every user, that we call a Qlient, through optical fibers (see figure 2). This allows for centralized routing procedures and asymmetrical distribution of hardware between a powerful Qonnector and limited Qlients. This corresponds to expected intermediate-term development of quantum hardware and its availability to end users. Below we describe precisely the abilities of a Qonnector and a Qlient node in our model.

Qonnector nodes are at the core of the Quantum City model. They abstract servers providing quantum services to end users. They are powerful nodes that can create, send and receive any state, and that are connected both classically and quantumly to a certain number of parties. We suppose a Qonnector has currently available state-of-the-art photonic capabilities, namely that it can create and manipulate single-qubit states as well as two and multiparty entangled states such as Bell pairs and GHZ states. We also suppose that Qonnectors have access to measurement devices allowing them to receive and measure qubit states and to perform probabilistic Bell state measurements on two qubits arriving simultaneously. Finally we suppose that Qonnectors have the ability to route photonic states arriving from a Qlient to another one and that they have access to usual classical computing power and classical Internet. In this work, Qonnectors also represent ground stations for satellite communication. We suppose that they are equipped with telescopes and measurement stations allowing them to receive and process photonic quantum states coming from a satellite. We also suppose that the Qonnector is able to couple the states coming from a satellite into a fiber and route them to any Qlient.

Qlient nodes represent the end users connected to the quantum internet. They are abstractions of private users that hold near-term photonic quantum communication devices. They are classically connected to the rest of the network through the classical Internet and have usual classical computing power. We suppose that

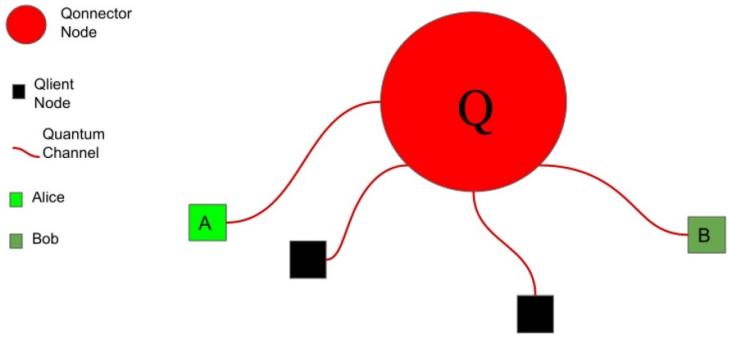

Figure 2. The Quantum City topology. It is a star-type photonic quantum network with a special node in the middle, the Qonnector, that has high quantum capabilities. Each end node (Qlient, such as Alice or Bob) has limited quantum hardware and is connected to the Qonnector through an optical fiber.

they have very limited quantum hardware capabilities, namely they manipulate one qubit at a time. More precisely they can create, send and manipulate any single-qubit photonic state as well as receive and measure it. Industrial-grade devices offering these capabilities are already available today or will become in the near future, and can be expected to become more suitable for wider use in the following years, thanks to advances for instance in photonic integration [53].

For more details on these nodes and how they are modeled in our simulations, please see [47].

2.2. Connecting quantum cities with satellites

Let us strat our analysis by detailing our model for the noise in satellite to ground quantum communication. Since atmospheric turbulence is a very complex phenomenon, the realization of an adequate model requires a choice of the effects that most severely affect the transmission. Here, we focus on atmospheric absorption and beam wandering effects.

In order to describe the impact of atmospheric propagation on the signal, we use a computer code called Lowtran [54], which is a Fortran code developed for the calculation of the transmittance and background radiance of the atmosphere. It is based on an empirical prediction scheme derived from lab measurements and provides a reasonably accurate estimation of atmospheric effects over a broad spectral interval ($\sim$0.25–28.5 μm). We briefly describe here the parameters that are included in the model of the atmosphere in Lowtran and refer to [54] for details. The atmosphere is represented by 33 horizontal layers between sea level and an altitude of 100 km. The total transmittance is computed as the product of different atmospheric effects, namely continuum absorption, aerosol extinction, molecular scattering and molecular absorption, the latter of which includes the influence of water vapor, ozone, nitric acid and other uniformly mixed gases. The program contains a few different representative atmospheric models based on geographical-seasonal characteristics (such as for tropical or mid-latitude environments) that encompass the variations of pressure, temperature, water vapor and ozone with altitude. It also accounts for several aerosol models that describe particular meteorological ranges such as an urban environment, a less severe rural setting or a more wind and humidity dependent maritime navy situation. Last, a few different visual ranges corresponding to different aerosol density models are considered as well [55].

In order to account for beam wandering, we used the model proposed in [56], which presents a rigorous treatment of beam wandering effects, one of the leading causes of losses in a free-space channel. Its main advantage lies in an analytical formulation of the probability distribution of the transmission coefficient (PDTC), a feature used to provide a computationally efficient software implementation of the model. The model has also been applied recently to the analysis of continuous-variable QKD over a satellite-to-ground channel [57]. While a subsequent, more complete model of atmospheric propagation for the satellite-to-ground case, including also scintillation and beam broadening effects, is described in [58], its much higher complexity makes it challenging to embed this model in NetSquid.

Beam wandering effects come from two main sources, namely the turbulence and the jitter due to the pointing error of the transmitter. The effects of beam wandering due to turbulence depend mostly on the size of the beam at the beginning of the propagation in the atmosphere and are determined by the refractive index structure constant C_n^2 which we will consider as fixed throughout the propagation. The satellite pointing jitter is, in turn, characterized by the standard deviation of the pointing error θ_p. The parameters that are necessary to physically describe the channel are the size of the transmitting and receiving stations and the properties of the atmosphere and the pointing system. The main characteristic of the receiving

station is the radius of the receiving telescope, which determines the proportion of the transmitted light that can be collected by the receiver.

The current code considers two possible configurations for this channel, namely the ground-to-ground free-space one (class FreeSpaceLossModel) and the satellite-to-ground one (class FixedSatelliteLossModel). The first one considers a horizontal channel, meaning that the entire propagation path is within the atmosphere and therefore will be affected by it. This can either be the case for direct communication between two ground stations or for a link between two drones or high altitude balloons carrying telescopes. In both cases, the C_n^2 value is indeed constant and will depend on the altitude of the link. For this configuration, the transmitter is characterized by the beam waist ω_0.

The second configuration considers a slant propagation path, only the last 10 km of which will be affected by the atmosphere. For this kind of links, a constant C_n^2 is more of an approximation since in reality it varies throughout the propagation path as it is a highly altitude dependent parameter. For this configuration, the transmitter is characterized by the divergence angle θ_d, a value related to the previously mentioned beam waist as follows: $\theta_d = \lambda/(\pi\omega_0)$.

As for the pointing error of the satellite, assuming that the position of the center of the transmitted beam with respect to the receiving aperture follows a normal distribution and is centered around the midpoint of the aperture, the PDTC will follow a log-negative Weibull distribution. The incidence of turbulence on beam wandering is less important for the satellite-to-ground case, becoming negligible in front of the beam wandering effects due to the pointing error θ_p.

The model assumes that each qubit is affected by the PDTC independently from the other qubits of the transmission. Despite being unrealistic since it neglects the dynamics of the atmosphere, which is considerably slower than the typical time delay between two qubits, it allows to provide a good insight of the average properties of the channel. In addition to this, the satellite-to-ground channel model assumes a fixed position for the satellite. This allows to give a first estimate of the performance of the channel when the satellite is on a given position in the sky, but it lacks the ability to provide information about a long-time operation on the channel. We take this into account externally by discretizing the orbit in 10 s intervals for which the satellite is considered as fixed and we then make a separate simulation for each trajectory.

In the following, we will use the satellite as a bacQbone node to connect two Quantum cities (see figure 1). We will suppose it is able to create and send single-qubit, BB84-type states with probability p_{qubit} at a time rate f_{qubit} as well as EPR states with probability p_{EPR} and a time rate f_{EPR} to two ground stations. We will use the terms 'raw rate' or 'QKD rate', or simply rate, over a network for the fraction $\frac{n_{\text{arrived}}}{n_{\text{sent}}}$, where n_{arrived} is the number of quantum states (either single-qubit photon states or EPR pairs) that actually arrived at the desired receiving nodes and n_{sent} is the number of quantum states that are sent over the network.

In this work, satellite links are used to connect fiber-based metropolitan networks. While experimental works [59] sometimes use photons at a wavelength of 850 nm, we note that fiber transmissivity for this wavelength is low, on the order of 4 dB km^{-1}. For that reason, we restrict our simulations to photons created in the telecom wavelength, 1550 nm, that have a much higher fiber transmissivity. We can then envision protocols in which photons are sent from a satellite, coupled into a fiber in the ground and sent to end users of the networks.

3. Simulation results

3.1. Setting and parameters

We consider the following network setting. We suppose that two European Quantum Cities, the city of Paris with five Qlients and the 'city' of the Netherlands with three Qlients are deployed, allowing for metropolitan scale quantum networking. We also suppose that satellites are travelling over Europe, following an orbit allowing to send qubit states to the Qonnectors (see figure 3). The Qlients localization corresponds to actual cities or laboratories. As in [47], the Paris Quantum City is composed of a Qonnector at the Sorbonne Université campus (SU), and5 nodes: Sorbonne Université (SU-Alice), Université Paris Cité campus (UPC-Bob), Orange Labs Châtillon (OR-Charlie), Télécom Paris (TP-Dina) and TGCC-CEA (CEA-Erika). The Dutch Quantum City is composed of a Qonnector at QuTech at the TU Delft campus and 3 Qlient nodes: Den Haag (Geralt), Rotterdam (Hadi) and Amsterdam (Fatou). Of course, please note that the choice of the Qonnector sites serves for illustration purposes only as these are urban areas, where installing optical ground stations with significant constraints would be challenging.

We recall below the baseline set of parameters used in our previous work [47] to simulate the performance of the Quantum City of Paris, which we will use here also to model sources, detectors and fiber links. These values are realistic with current or near term technology; see [47] and references therein for the justification of these parameters.

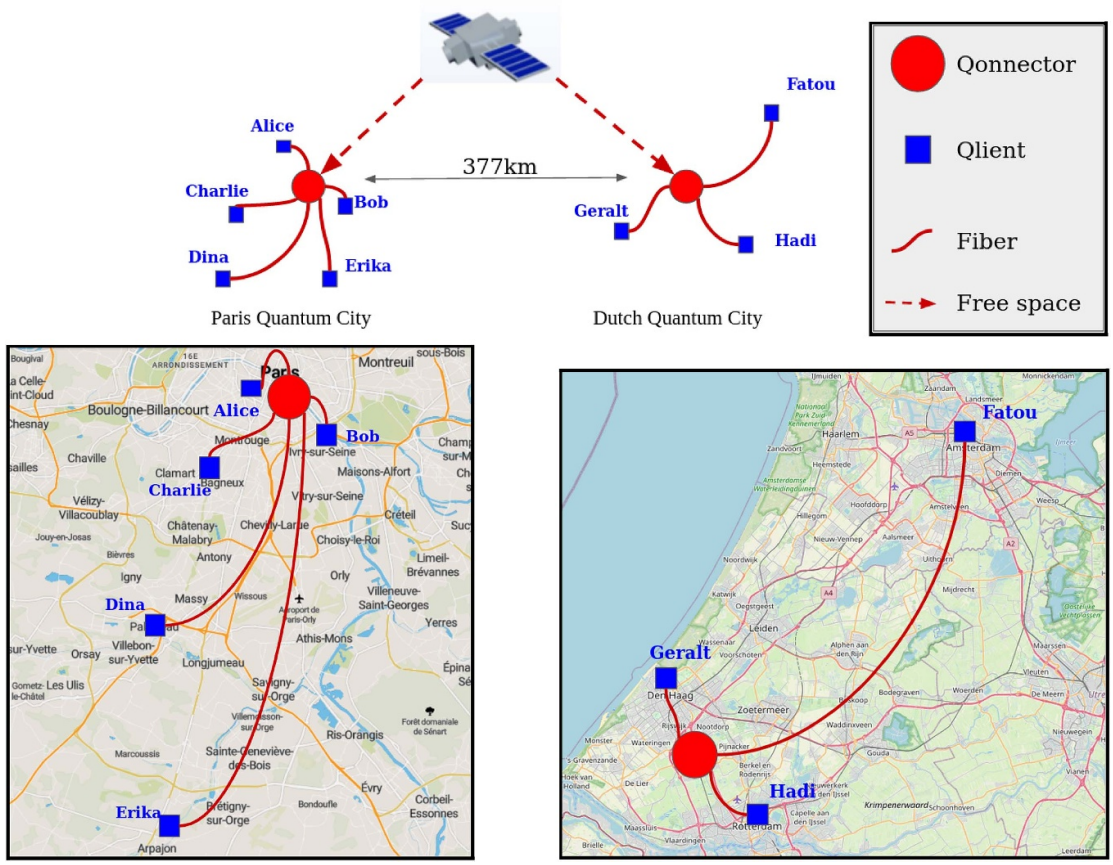

Figure 3. A satellite connecting Paris and Dutch Quantum Cities with downlinks only. Quantum City of Paris: five Qlients are connected through optical fibers to a Qonnector located in the SU campus. The length of the fiber links are 1 m for the link Alice-Qonnector, 3 km for the link Bob-Qonnector, 7 km for the link Charlie-Qonnector, 19 km for the link Dina-Qonnector and 31 km for the link Erika-Qonnector. Dutch Quantum City: three Qlients connected through optical fibers to a Qonnector placed in Delft. The length of the fiber are 54 km for the link Fatou-Qonnector, 9 km for the link Geralt-Qonnector and 13 km for the link Hadi-Qonnector.

f_{qubit}	80 MHz	Qubit creation attempt frequency
p_{qubit}	$8 \cdot 10^{-3}$	Success probability of creation of a qubit
p_{flip}	0	Flipping probability at the creation of a qubit
$p_{\text{crosstalk}}$	10^{-5}	Probability that the detector flips the outcome
f_{EPR}	80 MHz	EPR pair creation attempt frequency
p_{EPR}	10^{-2}	Success probability of the creation of an EPR pair
p_{BSM}	0.36	Probability that a Bell state measurement succeeds
p_{transmit}	0.81	Probability that transmitting a qubit succeeds
t_{gate}	1 ns	Time it takes to perform an operation on one qubit
p_{coupling}	0.81	Fiber coupling efficiency
η_{fiber}	0.18 dB km^{-1}	Fiber loss per kilometer
p_{dephase}	0.02	Phase flip probability in the fiber
p_{det}	0.95	Detector efficiency (Probability that a measurement succeeds)
R_{dark}	10^2 Hz	Dark count rate
Δt_{det}	100 ps	Detector detection gate

We point out that the rate at which single qubit states or EPR pairs are created depends strongly on the source model that we chose, namely spontaneous-parametric down-conversion (SPDC) in nonlinear crystals. This influences directly the rate at which entanglement can be created between different nodes of our network. This parameter, like all the others, can be tuned freely in our code for each source to match an actual source. For simplicity, we chose in this work to have the same qubit creation rates for the Qonnector and satellite sources. This is why we focus on the rate, in bit per attempt, at which protocols are performed instead of the throughput in bits per second. This gives a less source dependent view on the performance of the communication protocols that we study.

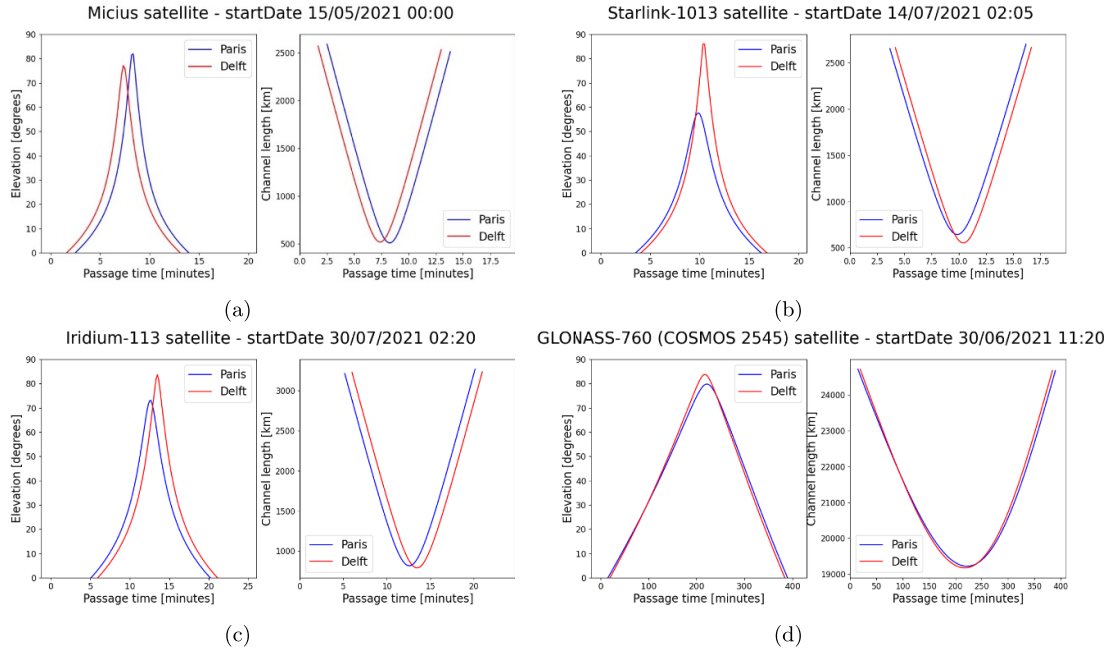

Figure 4. Elevation and distance to Paris and Delft of the (a) Micius, (b) Starlink, (c) Iridium and (d) Cosmo satellites in the time frame considered.

Note that we chose to simulate all protocols, including BB84, using single photons generated through SPDC while traditional methods to perform the BB84 protocol use weak coherent states and decoy methods, or more recently continuous-variable states. This choice is due to a limitation in our network simulator, NetsQuid, that is not able to simulate weak coherent states or continuous variable states. Using single-photon based BB84 allowed us to compare it fairly with the other QKD protocols. Moreover, it can be envisioned that future nodes of quantum networks will integrate solid-state memories, creating photonic states via SPDC, which corresponds to our model.

Using real live data from n2yo [60], a tracking website for satellites, and the orekit library [61], a low level space dynamics library, we are able to find satellites in different orbits and to track down the precise time frame where they would pass over Europe. This also gives us other useful information such as the elevation of the satellite as well as the distance between the satellite and our ground stations at each point in time. In the following we will focus on four different satellite orbits: the QSS (Micius) orbit that was used in [59], the Starlink-1013 orbit, the Iridium-113 orbit and the Cosmos-2545 orbit and we focus on a time frame where the elevation of the satellites allows for quantum communication (set here at 20 degrees). The first two considered are low Earth orbit (LEO) satellites evolving at around 550 km above Earth, with slightly different orbits: the Micius orbit passes exactly above Paris while the Starlink orbit passes next to it. The Iridium satellite is higher, around 800 km above Earth. Last, the Cosmos satellite is a middle Earth orbit (MEO) satellite, at around 19 000 km above Earth.

In figure 4 we show the elevation and the distance to the ground station for these satellites. We point out that our code is modular, accessible on GitHub [48, 49] and that any satellite can be investigated like we do in the following.

3.2. Simple downlink scenario: choosing a satellite

To test our model, we first simulate a simple downlink scenario between each of the satellites and the Qonnector from Paris. This will allow us to choose the satellite that is most suited for quantum communication.

The downlink scenario goes as follows: for each point in the orbit where the satellite's elevation is over 20 degrees, the satellite starts sending BB84 states to the Qonnector in Paris for one second while recording the time stamp of each state. The Qonnector receives, measures the states and records the measurement outputs. We can thus estimate the rate, i.e. the number of states received over the number of states sent, which also corresponds to the link efficiency at this point in the orbit. We average this over ten runs to get a better

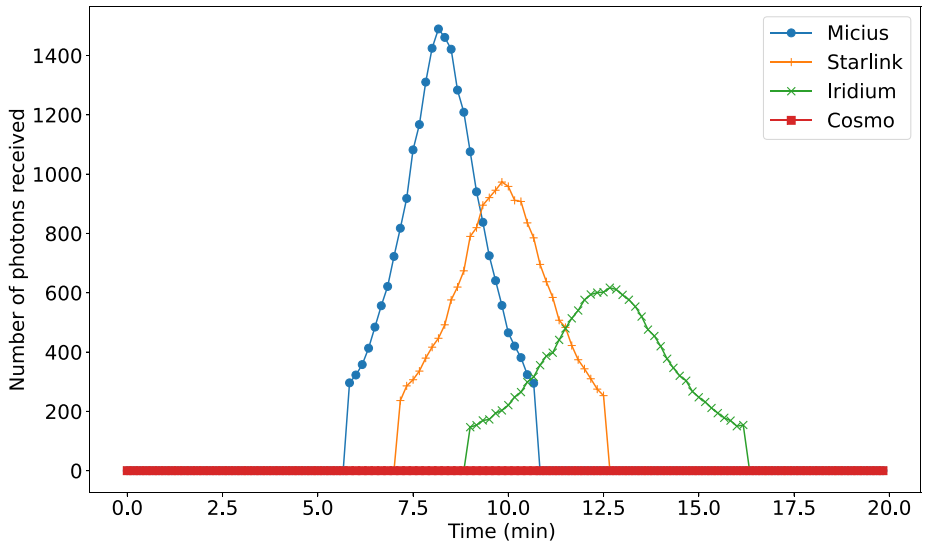

Figure 5. Comparison of the average number of photons received at the Paris Qonnector for the four satellites considered for approximately 6000 photons sent by the satellite at each point of its orbit. For this simulation we suppose there are no aerosols in the atmosphere and we set the aperture radius of the receiving telescope at 1 m, the beam waist divergence at 5 μrad and the pointing error at 0.5 μrad.

Table 1. Maximum rate for the four satellites. The maximum rate is the rate, i.e. the number of qubits received at the ground station over the number of qubits sent from the satellite, when the satellite is the closest to the ground station.

Satellite	Maximum rate
Micius	0.238
Starlink	0.157
Iridium	0.101
Cosmo	0

estimate. After this step is finished we move on to the next point in the orbit, ten seconds later. We show the result in figure 5 and in table 1 for a given set of parameters.

As expected, we observe that distance and elevation of the satellite impact the number of photons that arrive at the ground station. For example, we can see that none of the photons sent by the Cosmo satellite arrives at the Earth. The reason for this is that MEO satellites, while having the advantage of having a longer time frame during which the elevation allows for quantum communication than LEO satellites, are too far for single-photon states to arrive at a precise point on Earth due to the combined effects of pointing errors and beam wandering. It follows that this is even more challenging for geostationary satellites, which are at a height of 36 000 km above ground and have the significant advantage of always visible by a given ground station. As it is located further than the other two satellites, the Iridium satellite has a lower rate, but a longer exploitation time. We thus emphasize the well-known trade-off in satellite communication between distance of the satellite to the Earth and time frame in which we can use it, which we will discuss in more detail in section 5. The Micius and Starlink satellites are performing better but as can be seen in figure 4(b), the elevation angle of Starlink with respect to the Paris ground station is lower than the one of Micius. This means Starlink does not pass exactly above Paris, which causes a drop in the rate.

3.3. Influence of the parameters

As detailed in section 2.2, our loss model allows us to analyze the effect of a few important parameters of satellite communication, namely the aperture radius of the receiving telescope, the beam waist divergence, the pointing error and the aerosol model, which affect directly the atmospheric transmittance. In this section we study the effect of these different parameters on the rate in the downlink scenario. Based on the previous analysis, we chose to focus on the Micius satellite for the rest of this section as it exhibits the highest rate with the Paris node. When studying a parameter, we fix the other ones to what we expect to be the best value achievable in the near future: an aperture radius of the receiving telescope of 1 m, a beam waist divergence at 5 μrad and a pointing error at 0.5 μrad. We also suppose that the turbulence induced by beam-wandering is negligible with respect to the pointing error [57].

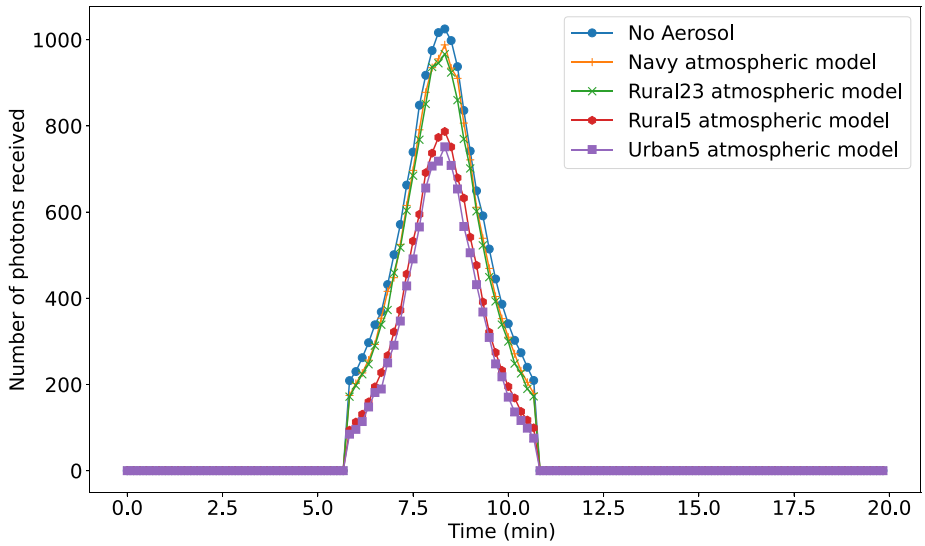

Figure 6. Effect of different aerosol models on the number of photonic states arriving from the Micius satellite.

We start with a study of the atmospheric model. In section 2.2 we have detailed a few atmospheric models that have an effect on photonic communication in free-space, and that have different meteorological ranges. The meteorological range is usually defined as the length of atmosphere over which a beam of light travels before its luminous flux is reduced to 2% of its original value [54]. Here we will study the ideal case where there is no aerosol between the ground station and the satellite, the rural5 and rural23 models that correspond to ground stations in rural areas with a meteorological range of, respectively, 5 and 23 km, the urban5 model that correspond to a ground station close to a city and the navy model corresponding to a ground station in the middle of the sea.

In figure 6 we show the number of photons received at the ground station when considering these different atmospheric models. This simulation has been done similarly to the one in the previous section, meaning that BB84 states are sent by the satellite for each point of the orbit where the elevation of the satellite is over 20 degrees. As expected, we observe in the figure that the smaller the meteorological range, the more photons are lost in the atmosphere. However, as we will see in section 5, atmospheric parameters have more drastic effects on the photon transmission when we get closer to the ground as aerosols are mostly concentrated there.

We then study, using again the downlink scenario, the effect of modifying the other parameters included in our model. This study allows us to know what to expect from a specific setting and to identify the key parameters to improve future quantum communication. The results are shown in figure 7. We see that the transmitter parameters do not all have the same importance. A change of 5 μrad in the beam divergence angle (see figure 7(a)), has a drastic effect on the number of photons arriving at the ground station. On the other hand, the pointing error of the transmitter (see figure 7(b)) has to be multiplied by five in order to reduce the number of arriving photons by a half. We also see that increasing the aperture radius of the receiving telescope at the ground station by 20 cm can almost double the number of qubits successfully measured (see figure 7(a)). This parameter might be the easiest to improve in future experimental realizations. Finally, the coupling efficiency at the receiving telescope is an active field of research that we will study in more depth in a future work. We simply model it as a tunable constant for now (see figure 7(d)) so it has a linear influence on the number of photon received.

4. QKD between two qlients

We now embed this study in the context of quantum networks by showing the performance of satellite communication when linking two Quantum Cities. We study the achievable QKD rate between two Qlients respectively from the quantum city of Paris and the Dutch quantum city connected via the Micius satellite (see figures 3 and 4(a)). We will consider the baseline set of parameters from the previous section, namely no atmospheric turbulence, an aperture radius of the receiving telescope of 1 m, a beam divergence at 5 μrad and a pointing error at 0.5 μrad.

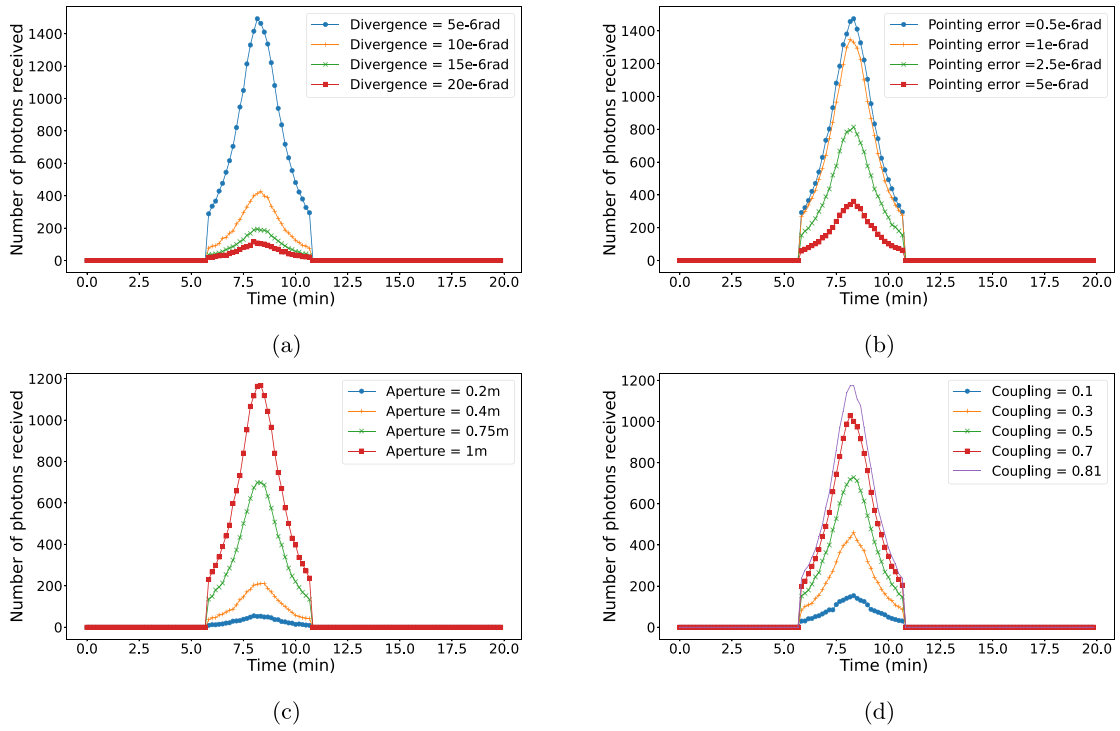

Figure 7. Number of photons received, from Micius satellite to ground station. In each plot, we fix non studied values as baseline values: no atmospheric turbulence, an aperture radius of the receiving telescope of 1 m, a beam divergence at 5 μrad and a pointing error at 0.5 μrad. The three subfigures show the effect of individually varying one of these parameters, while keeping the others constant: (a) the beam divergence angle θ_d, (b) the pointing error θ_p, (c) the aperture radius of the receiving telescope and (d) the coupling efficiency.

Let us imagine that one Qlient from the Paris Quantum City, say Bob, wants to share a secret key with a Qlient from the Dutch Quantum City, say Hadi, using a QKD protocol. There are different ways to achieve this functionality and we focus our analysis on two of them. For a more extensive study of the different ways of achieving QKD as well as some other protocols in a metropolitan network, see [47]. In the following we show the feasibility of two QKD scenarios, with a trusted and an untrusted node, and we then discuss their practical relevance.

4.1. Trusted satellite

The most standard way to achieve QKD between Bob and Hadi via the satellite is to perform BB84 between these nodes while trusting each of them not to reveal the keys they generate (figure 8). More precisely the satellite, when above one of the ground stations, performs two BB84 protocols in parallel to establish two keys with the Qonnectors of the two cities, k_{Paris} and k_{Delft}. At the same time the two Qlients establish secret keys, k_{Bob} and k_{Hadi} using the BB84 protocol with their Qonnector. Once all keys are created, the Paris Qonnector can send k_{Bob} as message to the satellite using k_{Paris} as key (with a classical encryption scheme such as one-time pad), and the satellite forwards the message to the Delft Qonnector using the key k_{Delft}, which subsequently sends the message to Hadi using the key k_{Hadi}. In the end, Bob and Hadi share k_{Bob}.

As in the analysis in the previous section, we simulate sending BB84 states to both ground stations and obtain the rate for the two satellite to ground links. We also simulate sending BB84 states from each Qlient to the Qonnectors. The parameters for all nodes are listed in section 3.1. We show the results of these simulations in figure 9 and table 2.

We observe, as expected, that the longer a photon has to travel in a fiber the lower is the rate. These number were computed with the satellite exactly above the Paris ground station, which explains the small difference in rate in the first two lines. In this scenario, the rate of the overall key distribution protocol is given by the minimum rate over all sublinks. Hence depending on the pair of nodes that want to establish a secure key, the limiting sublink can be either the satellite-to-ground link or the fiber link. For example if Hadi and Bob want to perform the QKD protocol considered here, their total rate is limited by the rate of the satellite-to-ground link. But if Erika and Fatou want to do the same, it is the fiber link between Fatou and her Qonnector that is most limiting. Note that the satellite-to-ground rate here is the rate when the satellite is at its optimal position, namely just above the ground stations. As an example of performance, with a source

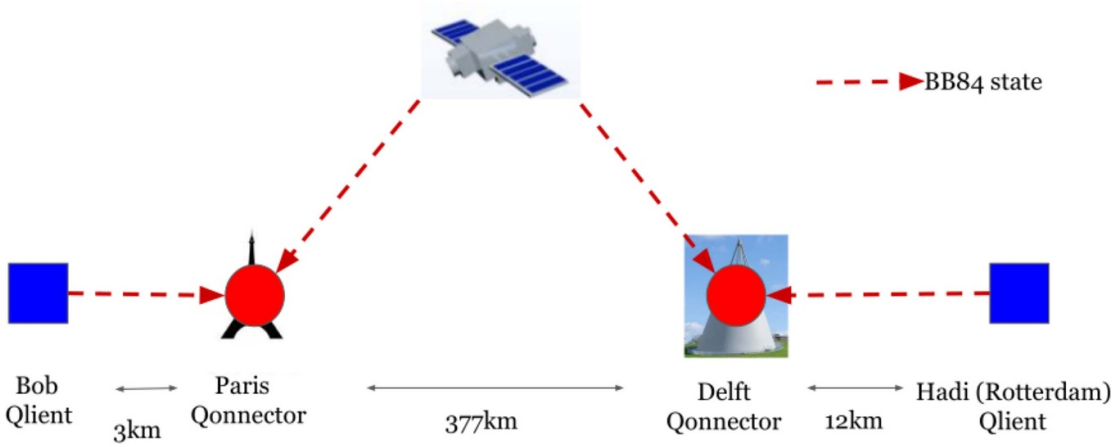

Figure 8. QKD between Bob and Hadi: all trusted node scenario. Here keys are generated between all different node pairs and are transfered as secret messages. In the end, Bob and Hadi share k_{Bob}.

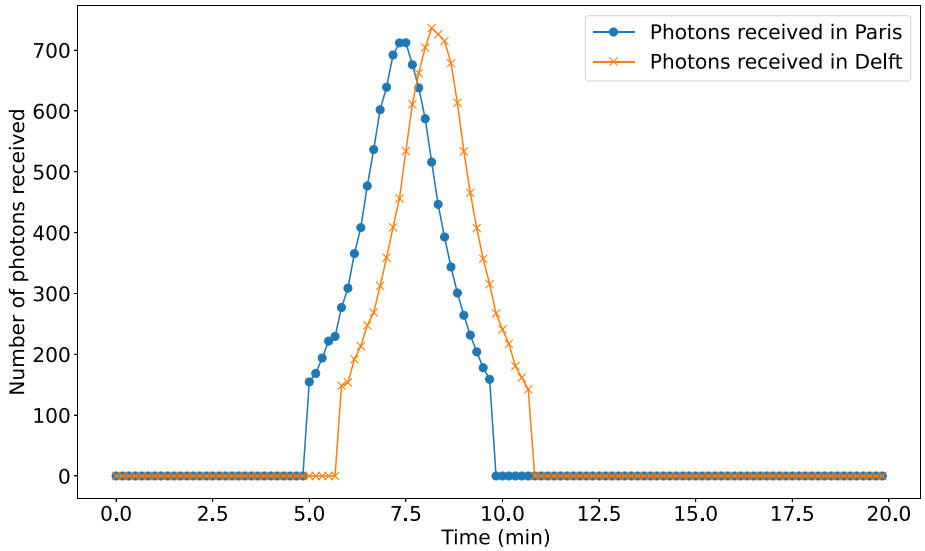

Figure 9. Average number of photons received in Paris and Delft for approximately 3000 photons sent from the satellite at each orbit point.

Table 2. Performance of the BB84 protocol between all nodes. The first two rows correspond to the satellite sending BB84 states to the two ground stations, and the other rows correspond to BB84 rates with each Qlient inside the two Quantum Cities.

Nodes involved	Rate (raw key bit per channel use)
Satellite − >Paris Qonn	0.238
Satellite − > Dutch Qonn	0.228
Alice − > Paris Qonn	0.423
Bob − > Paris Qonn	0.374
Charlie − > Paris Qonn	0.322
Dina − > Paris Qonn	0.180
Erika − > Paris Qonn	0.115
Fatou − > Dutch Qonn	0.043
Geralt − > Dutch Qonn	0.296
Hadi − > Dutch Qonn	0.253

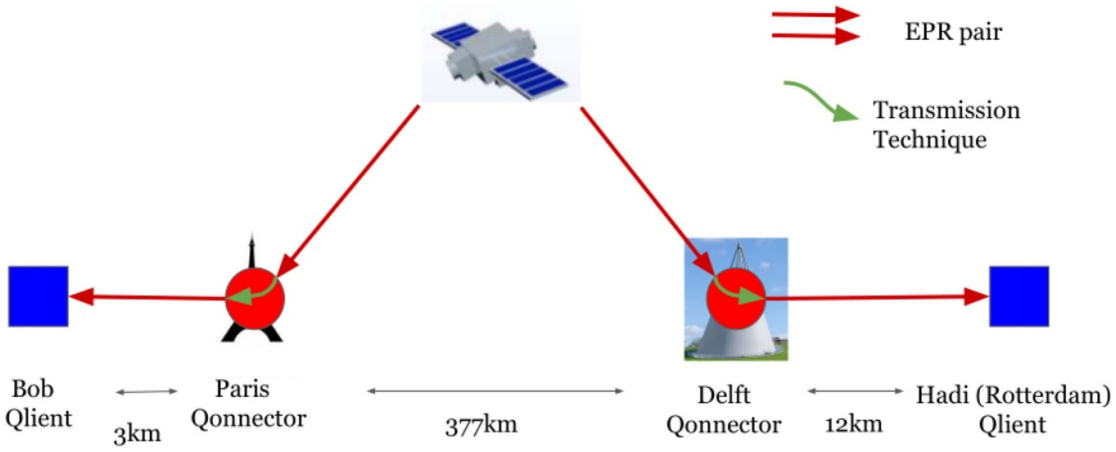

Figure 10. QKD between Bob and Hadi: untrusted nodes. Here the satellite performs the BBM92 protocol directly with the Qlients. The Qonnectors are used as transmitting stations that couple the photons arriving from the satellite into a fiber and send them to the Qlients.

rate of 80 MHz, the raw key rate at this point of the orbit is 1.7 Mbit s^{-1} for Bob and Hadi and 300 kbit s^{-1} for Erika and Fatou. We discuss how practical these values are in section 4.3. Note once more that in order for this scenario to securely create a key between two Qlients, all the nodes (Qonnectors and satellite) along the path between two Qlients have to be trusted.

4.2. Untrusted satellite

Another way to distribute a secret key between Hadi and Bob is to use an entanglement-based version of QKD, and in particular the BBM92 protocol [62]. This requires that an EPR pair is shared between the two Qlients. More specifically, in the context of Quantum Cities connected by a satellite, the protocol goes as follows (see figure 10): an EPR pair in the state $|\psi^-\rangle = \frac{1}{\sqrt{2}}(|01\rangle - |10\rangle)$ is created at the satellite and each qubit of the pair is sent towards two Qonnectors at the ground. It is then coupled into an optical fiber and transmitted to the Qlient who measures it. The Qlients keep the outcomes measured with the same timestamp to post-select the qubits that came from the same pair. These steps are performed for each point of the Micius orbit where the satellite elevation is above 20 degrees for both Qonnectors. The coupling of a photon coming from a satellite into a fiber succeeds with probability p_{transmit} that we fix to 81% [63]. Coupling photons arriving from a satellite into a fiber can be improved by using adaptive optics to correct atmospheric effects [64]. This parameter is of course freely tunable in our simulation.

Simulating the process described above for each point in the satellite orbit and averaging over tens of runs, we obtain the rate as the ratio between the number of pairs sent from the satellite and the number of pairs received by the Qlients. We show the results of simulations with different pairs of Qlients in figure 11 and table 3.

As before, in addition to the loss due to atmospheric perturbation between the satellite and the ground stations, the rate is affected by the distance photons have to travel in optical fibers from the Qonnectors to each Qlient. As expected the longer this distance is, e.g. for Erika and Fatou, the lower the rate is. This is also why the rate is similar for the two pairs of Qlients Bob & Hadi and Charlie & Geralt: the distance photons have to travel into fibers is comparable (see figure 3). With a source rate of 80 MHz , the raw key throughput would be 150 kbit s^{-1} for Hadi and Bob, and 14 kbit s^{-1} for Erika and Fatou.

We emphasize again that compared to this untrusted node scenario, the trusted node scenario as studied in the previous section has a higher rate, albeit at the cost of the additional security assumption that the Qonnector and satellite nodes are not under control of an adversary.

4.3. Realistic QKD

The above simulations illustrate the feasibility of QKD between two Quantum Cities separated by a few hundreds of kilometers. However this analysis assumes that the satellite is always visible by the ground stations. This is unrealistic since, since as we saw in section 2.2, the time span during which a satellite's elevation allows for quantum communication is only a few minutes. Considering this, in the trusted node scenario above, the total raw key established between the Micius satellite and the Paris ground station during

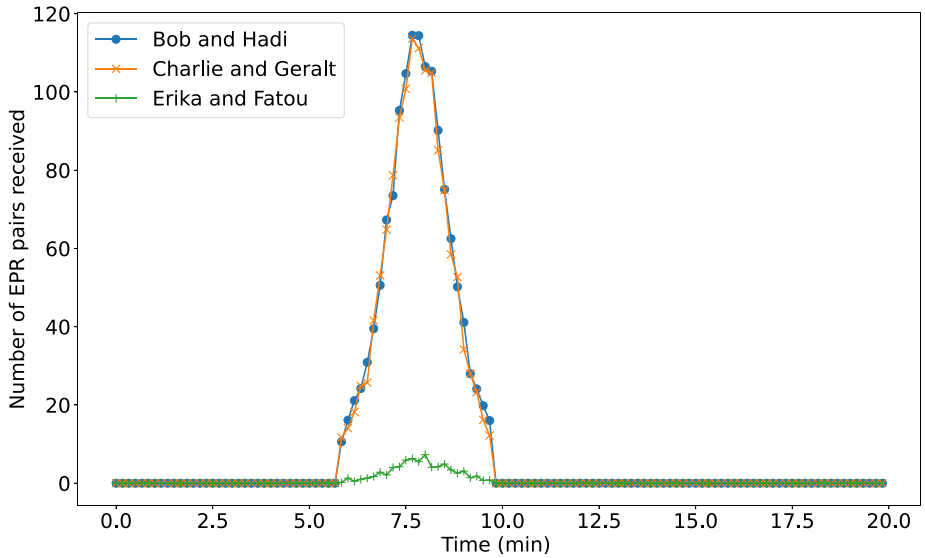

Figure 11. Average number of successfully transmitted EPR pairs from the Micius satellite to pairs of Qlients in the two Quantum Cities considered. For each point of the orbit we simulate sending approximately 650 EPR pairs from the satellite and average over ten rounds.

Table 3. Average rate for pairs of Qlients of the two Quantum Cities considered when the satellite is exactly in the middle of the two ground stations.

Qlient pairs	Rate (raw key bit per channel use)
Bob & Hadi	0.0183
Charlie & Geralt	0.0185
Erika & Fatou	0.0019

the whole passage of the satellite above Europe is of length 17 kbits on average. This limits significantly the amount of messages that can be securely sent between the two Qlients considered.

To overcome this limitation, a possible solution is to use multiple passages of a satellite over several days to create and store keys at the ground stations. These keys can be established, for instance, using one of the two scenarios presented above. They can subsequently be used to establish a secure communication channel between the Qlients. This is useful in scenarios where relatively small amount of shared secret key is required. The secure storage of the key material at the nodes also needs to be considered in this case.

This solution may not however apply to quantum communication protocols beyond QKD, where nodes need to be remained entangled for long periods of time. Constellations of satellites orbiting around the Earth offer an alternative solution. In this case, once a satellite is out of reach for quantum communication, another suitable satellite in the constellation can be used to continue the key generation. Finding the optimal orbit height and the optimal number of satellites on this orbit is a complex question and detailed studies are required to address all the associated challenges; see for example [43].

Some other issues that may directly affect the key rate have not been taken into account in this study. For example, we neglected here the variations of atmospheric turbulence with the position of the Qonnector and the conditions at the time of the key establishment, which play a central role in satellite communication. Moreover, in our simulations we considered the wavelength of the photon to be 1550 nm, which is convenient for coupling them with telecom equipment on the ground. In the Micius experiment [59], the operational wavelength is 850 nm, which would also alter the results. Finally, as we focus in study on the feasibility of satellite communication in the context of quantum networks, we have neglected entirely the problem of scheduling operations at each node. In realistic scenarios, the Qonnector and satellite nodes may not be able to perform operations in parallel and thus would have to store qubits until their processing unit is available. Including the effect of quantum memories and synchronization techniques is a crucial follow-up work of the present analysis.

Even without covering all aspects of a full quantum communication network, we hope that this study shows the possibilities and limitations of satellite communication to link local networks. According to our simulations, current technologies could already allow for interesting applications between distant cities, as we discuss in the next section.

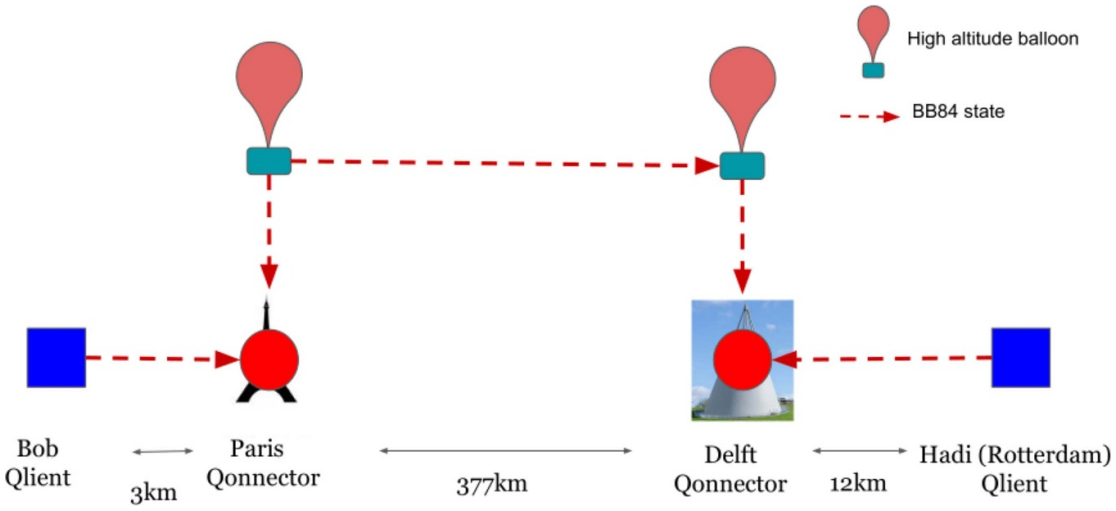

Figure 12. A trusted node QKD scenario between two Qlients using two high-altitude balloons over the Qonnectors. We assume that the balloons are located directly above each Qonnector.

Table 4. Atmospheric transmittance for different heights above the ground.

Height	T_{atm}
10 km	0.96 753
5 km	0.85 255
1 km	0.26 363

5. Discussion

5.1. Comparison with ground-based and balloon-based communication

As we mentioned in the introduction, current quantum repeater technologies do not allow for practical key rates over the distances that we consider here. Assuming the realization of a quantum repeater link over about 50 km in the next few years, since the distance between the Dutch Quantum City and the one of Paris is 377 km, we would need between five and ten repeater nodes. Important quantum repeater parameters include the overall efficiency of the link (comprising the probability of photon emission, the storage-and-retrieval efficiency, the coupling and detection efficiencies), and the probability of success of the swapping operation via the Bell state measurement. Promising technologies based on various platforms [26, 27] or alternative models such as all photonic quantum repeaters [65] are presently under intense investigation to achieve this goal.

In parallel, an alternative technological path that could be envisioned is the use of drones or high-altitude balloons. Let us imagine a QKD scenario using two stationary high-altitude balloons above the Paris and Dutch Qonnectors. As we show in figure 12, this configuration is the same as the one considered in section 4.1, whereby secret keys are established between each pair of nodes and used to transmit as secret message the final private key between the two Qlients. In the rest of this section, we explore some key parameters in order to obtain an estimate of the key rate in this scenario.

Using the free-space loss model described in section 2.2 and the parameters of section 3.1, we obtain the key rate between the two balloons and between each balloon and the Qonnector using our simulation tools. First, the height of the balloons is of crucial importance because the atmospheric transmittance gets smaller when closer to the ground as we show in table 4. Moreover, the aerosols are concentrated in the lower layers of the atmosphere and thus have a much higher impact on the atmospheric transmittance when the photon path is closer to the ground as we show in table 5. We recall that the rural5 and rural23 aerosol models correspond to ground stations in rural areas with a meteorological range of, respectively, 5 and 23 km, and the urban5 aerosol model corresponds to a ground station close to a city.

For our study here, we fix the balloons height at 10 km and suppose that there are no aerosols in the atmosphere. We also suppose that the aperture radius of the receiving telescope in the balloons is 40 cm, and we fix the beam divergence at 5 μrad and the pointing error at 0.5 μrad. We compute separately the horizontal atmospheric transmittance between the two balloons and the vertical atmospheric transmittance

Table 5. Atmospheric transmittance at an altitude of 10 km and 1 km for different aerosol models.

Aerosol model	T_{atm} at 10 km	T_{atm} at 1 km
No aerosol	0.96 753	0.26 363
rural23 model	0.90 658	1.6209×10^{-7}
rural5 model	0.90 647	1.4159×10^{-31}
urban5 model	0.906 622	3.2276×10^{-38}

Table 6. BB84 rate for balloon-to-balloon communication for different values of C_n^2. The balloons are separated by 377 km and are located at a height of 10 km.

Value of C_n^2	Rate
0	0.138
10^{-17}	0.079
10^{-16}	0.014
10^{-15}	0.001
10^{-13}	1×10^{-5}

Table 7. BB84 rate for every sublink across the path between Bob and Hadi.

Sublink	Rate
Bob $->$ Paris Qonn	0.374
Paris Drone $->$ Paris Qonn	0.463
Paris Drone $->$ Dutch Drone	0.079
Dutch Drone $->$ Dutch Qonn	0.463
Dutch Qonn $->$ Hadi	0.253

between the balloon and the ground station (around 0.9). As the free-space communication happens in the atmosphere, we can no longer neglect the effect of the refractive index structure constant C_n^2 as it was done in the satellite case. In reality, the value of C_n^2 also depends on the height of the high-altitude balloons. As we show in table 6, this value has a drastic effect on the key rate between the two balloons. In what follows we choose an optimistic yet non-zero value for C_n^2 between the two balloons, namely 10^{-17}. For the balloon-to-Qonnector links we fix C_n^2 at 10^{-15} and take the aperture of the receiving telescope at the Qonnector to be 1 m. In table 7 we show the rate for all the sublinks between Bob and Hadi.

The QKD rate of this scenario is thus limited by the drone-to-drone link and would be 0.079 bits per attempt for Bob and Hadi. Note that this gives us only a first estimate of the BB84 rate between two Qlients in Quantum Cities linked with high-altitude balloons. It shows however the feasibility of such free-space links, which could come as a more accessible solution to perform quantum communication when satellites are not available. Theoretically, two balloons at 10 km altitude can be separated by a maximum 714 km and still be visible in the horizon. We leave a more detailed study of this kind of high-altitude balloon links for future work.

5.2. Towards quantum internet applications

Once entanglement is generated between the Qonnectors of our two Quantum cities, several applications, beyond QKD, becomes available to the Qlients. For instance, as we detailed in [47], sharing a GHZ state, $\frac{|0\rangle^{\otimes n}+|1\rangle^{\otimes n}}{\sqrt{2}}$ [66], to the Qlients and processing the measurement outcomes enables conference key agreement protocols [67, 68], the multipartite counterpart of QKD allowing n parties to get a secure shared key, or anonymous transmission [11] and electronic voting [12] with high security and privacy guarantees. Through Bell state measurements and local operations, two GHZ states and a Bell pair can be transformed into a bigger GHZ state as we show in figure 13. For more information about graph state manipulation, see e.g. [14, 69]. These techniques are interesting for scaling up quantum networking applications, including for satellite quantum communication in the long run.

The implementation of protocols relying on multipartite entanglement in a realistic adversarial framework typically relies on performing multiple rounds of state verification [10] in between rounds of actual use of the state. For this, high-fidelity states need to be generated and routed efficiently through the network. This is quite challenging with present technology. As explained in detail in [47], photonic GHZ states are created by simultaneously creating Bell pairs by spontaneous parametric down conversion that are then entangled using fusion gates [70]. All these processes are probabilistic and this makes the probability of

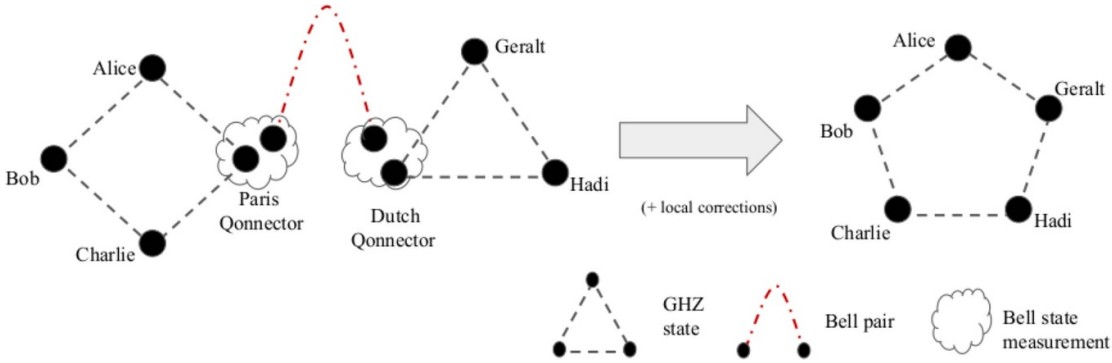

Figure 13. By making Bell state measurements and local operations, two GHZ states generated in Paris and the Netherlands can be transformed into one single shared GHZ state, consuming one Bell pair shared between the two metropolitan networks.

succeeding in creating a GHZ state quite low: on the order of 10^{-3} for 3 or 4 qubits GHZ states and 10^{-5} for 5 or 6 qubits GHZ state. State generation using single-photon sources may eventually improve these rates.

Our Qloud architecture is compatible with the deployment of such applications that will become available as technology progresses, and with other ones yet to be discovered that will rely on equivalent resources. Considering upgradability to accommodate advanced applications in the design of near-term quantum networks is important such that the developed technology can be efficiently used at all network stages. We also remark that the Qloud architecture is convenient for new users to join as they only has to connect to their Qonnector in a Quantum City. Future work will explore how communication between bacQbone nodes could be optimized to facilitate communication of two Qlients in distant Quantum Cities, for example Dina and Alice in figure 1.

6. Conclusion

In this work, we have studied the feasibility of satellite quantum communication between two Quantum Cities in Europe through the development and use of a simulation library for the NetSquid quantum-network simulator. Through these simulations, we were able to perform parameter exploration of quantum communication from satellite to ground stations, using real satellite data, by computing the transmissivity for each individual photon. Our code is available on GitHub [48, 49] and is modular. We then embedded this analysis in a quantum network setting, to explore the relevance of satellite communication in concrete scenarios. We showed the performance of two different QKD configurations in a specific realistic setting linking two European cities. The underlying Qloud architecture shown in figure 1 minimizes end user hardware while facilitating routing of entanglement, and also allowing for several alternatives for creating correlation between the users. We also discussed alternatives to satellite communication for connecting different Quantum Cities, such as high-altitude balloons. Combinations of terrestrial, free-space and satellite links will likely be required for the realization of the full-scale Quantum Internet. We believe that simulation tools like the ones developed for this work are instrumental for assessing the necessity and gain of deploying such resource-intensive infrastructures, considering all relevant trade-offs in performance, service availability, security, etc for promising quantum networking use cases.

Data availability statement

The data that support the findings of this study are openly available at the following URL/DOI: https://github.com/rajayehia/quantumcity.

Acknowledgments

This Project has received funding from the European Union's Horizon Europe research and innovation program under the Grant Agreement Nos 101102140 (QIA) and 101114043 (QSNP), and under the Project QUANGO (Grant No. 101004341). We acknowledge support from the French National Research Agency (ANR) through the project SoLuQS as well as the Dutch National Growth Fund, as part of the Quantum Delta NL programme. This work was also supported by the JST Moonshot R&D program under Grants JPMJMS226C

ORCID iDs

Raja Yehia https://orcid.org/0000-0002-7843-7398
Eleni Diamanti https://orcid.org/0000-0003-1795-5711

References

[1] Wehner S, Elkouss D and Hanson R 2018 Quantum internet: a vision for the road ahead *Science* **362** eaam9288
[2] Scarani V, Bechmann-Pasquinucci H, Cerf N J, Dušek M, Lütkenhaus N and Peev M 2009 The security of practical quantum key distribution *Rev. Mod. Phys.* **81** 1301–50
[3] Ganz M 2009 Quantum leader election *Quantum Inf. Process.* **16** 10
[4] Hillery M, Bužek V and Berthiaume A 1999 Quantum secret sharing *Phys. Rev.* A **59** 1829–34
[5] Brassard G 2003 Quantum communication complexity *Found. Phys.* **33** 1593–616
[6] Fitzsimons J 2016 Private quantum computation: an introduction to blind quantum computing and related protocols *npj Quantum Inf.* **3** 11
[7] Dunjko V, Fitzsimons J F, Portmann C and Renner R 2014 Composable Security of Delegated Quantum Computation *Advances in Cryptology – Asiacrypt 2014 ed P* Sarkar and T Iwata (Springer) pp 406–25
[8] Danos V, D'Hondt E, Kashefi E and Panangaden P 2007 Distributed measurement-based quantum computation Electronic Notes in Theoretical Computer Science *Proc. 3rd Int. Workshop on Quantum Programming Languages (QPL 2005)* vol 170 pp 73–94
[9] Shettell N, Hassani M and Markham D 2022 Private network parameter estimation with quantum sensors preprint (https://doi.org/10.48550/arXiv.2207.14450)
[10] Pappa A, Chailloux A, Wehner S, Diamanti E and Kerenidis I 2011 Multipartite entanglement verification resistant against dishonest parties *Phys. Rev. Lett.* **108** 12
[11] Unnikrishnan A, MacFarlane I, Richard Y, Diamanti E, Markham D and Kerenidis I 2018 Anonymity for practical quantum networks *Phys. Rev. Lett.* **122** 11
[12] Centrone F, Diamanti E and Kerenidis I 2021 Quantum protocol for electronic voting without election authorities *Phys. Rev. Appl.* **18** 014005
[13] Murta G, Grasselli F, Kampermann H and Bruß D 2020 Quantum conference key agreement: a review *Adv. Quantum Technol.* **3** eabe0395
[14] Meignant C, Markham D and Grosshans F'eric 2019 Distributing graph states over arbitrary quantum networks *Phys. Rev.* A **100** 052333
[15] Bugalho L, Coutinho B C, Monteiro F A and Omar Y 2023 Distributing multipartite entanglement over noisy quantum networks *Quantum* **7** 920
[16] IETF Quantum Internet Research Group Architectural principles for a quantum internet (available at: https://datatracker.ietf.org/doc/draft-irtf-qirg-principles/)
[17] Koduru Joshi S K, Aktas D, Wengerowsky S, Lončarić M, Neumann S P, Liu B, Scheidl T, Currás Lorenzo G C, Samec Ž, Kling L and Qiu A 2020 A trusted node-free eight-user metropolitan quantum communication network *Sci. Adv.* **6** eaba0959
[18] Chen Y-A *et al* 2021 An integrated space-to-ground quantum communication network over 4,600 kilometres *Nature* **589** 214–9
[19] Pirandola S, Laurenza R, Ottaviani C and Banchi L 2017 Fundamental limits of repeaterless quantum communications *Nat. Commun.* **8** 15043
[20] Takeoka M, Guha S and Wilde M M 2014 Fundamental rate-loss tradeoff for optical quantum key distribution *Nat. Commun.* **5** 5235
[21] Briegel H-J, Dür W, Cirac J I and Zoller P 1998 Quantum repeaters: the role of imperfect local operations in quantum communication *Phys. Rev. Lett.* **81** 5932–5
[22] Munro W J, Azuma K, Tamaki K and Nemoto K 2015 Inside quantum repeaters *IEEE J. Sel. Top. Quantum Electron.* **21** 78–90
[23] Sangouard N, Simon C, de Riedmatten H and Gisin N 2011 Quantum repeaters based on atomic ensembles and linear optics *Rev. Mod. Phys.* **83** 33–80
[24] Azuma K, Economou S E, Elkouss D, Hilaire P, Jiang L, Hoi-Kwong L, and Tzitrin I 2022 Quantum repeaters: from quantum networks to the quantum internet (arXiv:2212.10820)
[25] Bhaskar M K *et al* 2020 Experimental demonstration of memory-enhanced quantum communication *Nature* **580** 60–64
[26] Pompili M *et al* 2021 Realization of a multinode quantum network of remote solid-state qubits *Science* **372** 259–64
[27] Lago-Rivera D, Grandi S, Rakonjac J V, Seri A and de Riedmatten H 2021 Telecom-heralded entanglement between multimode solid-state quantum memories *Nature* **594** 37–40
[28] Rozpedek F, Yehia R, Goodenough K, Ruf M, Humphreys P C, Hanson R, Wehner S and Elkouss D 2019 Near-term quantum-repeater experiments with nitrogen-vacancy centers: overcoming the limitations of direct transmission *Phys. Rev.* A **99** 052330
[29] Ruf M, Wan N H, Choi H, Englund D and Hanson R 2021 Quantum networks based on color centers in diamond *J. Appl. Phys.* **130** 070901
[30] Avis G, da Silva F F, Coopmans T, Dahlberg A, Jirovská H, Maier D, Rabbie J, Torres-Knoop A and Wehner S 2022 Requirements for a processing-node quantum repeater on a real-world fiber grid (arXiv:2207.10579)
[31] Bonato C, Tomaello A, Da Deppo V, Naletto G and Villoresi P 2009 Feasibility of satellite quantum key distribution *New J. Phys.* **11** 045017
[32] Bourgoin J-P *et al* 2013 A comprehensive design and performance analysis of low earth orbit satellite quantum communication *New J. Phys.* **15** 023006
[33] Schmitt-Manderbach T *et al* 2007 Experimental demonstration of free-space decoy-state quantum key distribution over 144 km *Phys. Rev. Lett.* **98** 010504
[34] Nauerth S, Moll F, Rau M, Fuchs C, Horwath J, Frick S and Weinfurter H 2013 Air-to-ground quantum communication *Nat. Photon.* **7** 382–6
[35] Wang J-Y *et al* 2013 Direct and full-scale experimental verifications towards ground–satellite quantum key distribution *Nat. Photon.* **7** 387–93
[36] Vallone G, Bacco D, Dequal D, Gaiarin S, Luceri V, Bianco G and Villoresi P 2015 Experimental satellite quantum communications *Phys. Rev. Lett.* **115** 040502

[37] Günthner K et al 2017 Quantum-limited measurements of optical signals from a geostationary satellite *Optica* **4** 611
[38] Chao-Yang L, Cao Y, Peng C-Z and Pan J-W 2022 Micius quantum experiments in space *Rev. Mod. Phys.* **94** 035001
[39] Liao S-K et al 2017 Satellite-to-ground quantum key distribution *Nature* **549** 43–47
[40] Yin J et al 2020 Entanglement-based secure quantum cryptography over 1, 120 kilometres *Nature* **582** 501–5
[41] Ren J-G et al 2017 Ground-to-satellite quantum teleportation *Nature* **549** 70–73
[42] Liorni C, Kampermann H and Bruß D 2021 Quantum repeaters in space *New J. Phys.* **23** 053021
[43] Khatri S, Brady A J, Desporte R A, Bart M P and Dowling J P Spooky action at a global distance: analysis of space-based entanglement distribution for the quantum internet *npj Quantum Inf.* **7** 2021
[44] Boone K, Bourgoin J-P, Meyer-Scott E, Heshami K, Jennewein T and Simon C 2015 Entanglement over global distances via quantum repeaters with satellite links *Phys. Rev.* A **91**
[45] Coopmans T et al 2021 Netsquid, a network simulator for quantum information using discrete events *Commun. Phys.* **4** 1–15
[46] Netsquid website (available at: https://netsquid.org/)
[47] Yehia R, Neves S, Diamanti E, and Kerenidis I 2022 Quantum city: simulation of a practical near-term metropolitan quantum network (arXiv:2211.01190)
[48] Yehia R Github repository for the netsquid simulation modules (available at: https://github.com/rajayehia/quantumcity)
[49] Schiavon M and Netsquid-freespace T C (available at: https://github.com/matteoschiav/netsquid-freespace)
[50] Moll F et al 2019 Stratospheric QKD: feasibility analysis and free-space optics system concept *Quantum Technologies and Quantum Information Science* ed V M T Gruneisen, M Dusek, J G Rarity and P M Alsing (SPIE)
[51] Vu M Q, Pham T V, Dang N T and Pham A T 2020 Design and performance of relay-assisted satellite free-space optical quantum key distribution systems *IEEE Access* **8** 122498–510
[52] Chu Y, Donaldson R, Kumar R and Grace D 2021 Feasibility of quantum key distribution from high altitude platforms *Quantum Sci. Technol.* **6** 035009
[53] Moody G et al 2022 roadmap on integrated quantum photonics *J. Phys: Photon.* **4** 012501
[54] Kneizys F X, Shettle E P, Abreu L W, Chetwynd J H and Anderson G P 1988 *Users Guide to Lowtran* vol 7 (Air Force Geophysics Laboratory)
[55] Kneizys F X 1978 Atmospheric transmittance and radiance: the lowtran code *Optical Properties of the Atmosphere* vol 142 (International Society for Optics and Photonics) pp 6–8
[56] Vasylyev D Y, Semenov A A and Vogel W 2012 Toward global quantum communication: Beam wandering preserves nonclassicality *Phys. Rev. Lett.* **108** 220501
[57] Dequal D, Trigo Vidarte L, Roman Rodriguez V, Vallone G, Villoresi P, Leverrier A and Diamanti E 2021 Feasibility of satellite-to-ground continuous-variable quantum key distribution *npj Quantum Inf.* **7** 3
[58] Vasylyev D, Vogel W and Moll F 2019 Satellite-mediated quantum atmospheric links *Phys. Rev.* A **99** 053830
[59] Liao S-K et al 2018 Satellite-relayed intercontinental quantum network *Phys. Rev. Lett.* **120** 030501
[60] (Available at: www.n2yo.com/)
[61] Orekit library (available at: www.orekit.org/)
[62] Bennett C H, Brassard G and David Mermin N 1992 Quantum cryptography without bell's theorem *Phys. Rev. Lett.* **68** 557–9
[63] Klein B J and Degnan J J 1974 Optical antenna gain 1: transmitting antennas *Appl. Opt.* **13** 2134–41
[64] Marulanda Acosta V, Dequal D, Schiavon M, Montmerle-Bonnefois A, Lim C B, Conan J-M and Diamanti E 2024 *New J. Phys.* **26** 023039
[65] Azuma K, Tamaki K and Hoi-Kwong L 2015 All-photonic quantum repeaters *Nat. Commun.* **6** 6787
[66] Greenberger D M, Horne M A and Zeilinger A 1989 *Going Beyond Bell's Theorem* (Springer) pp 69–72
[67] Hahn F, de Jong J and Pappa A 2020 Anonymous quantum conference key agreement *PRX Quantum* vol 1
[68] Murta G, Grasselli F, Kampermann H and Bruß D 2020 Quantum conference key agreement: a review *Adv. Quantum Technol.* **3** 2000025
[69] Dahlberg A, Helsen J and Wehner S 2020 How to transform graph states using single-qubit operations: computational complexity and algorithms *Quantum Sci. Technol.* **5** 045016
[70] Bouwmeester D, Pan J-W, Daniell M, Weinfurter H and Zeilinger A 1999 Observation of three-photon Greenberger-Horne-Zeilinger entanglement *Phys. Rev. Lett.* **82** 1345